



One-step synthesis of water-soluble graphitic carbon nitride nanosheets with enhanced visible-light photocatalytic activity

Huiya Wang^a, Keqiang Ding^{a,*}, Danping Shao^b, Guoqiang Pan^b

^aSchool of Environmental Engineering, Nanjing Institute of Technology, No. 1 Hongjing Avenue Jiangning Science Park, Nanjing, Jiangsu CN211167, China, emails: dingkq@njit.edu.cn (K.Q. Ding), whyplgl@njit.edu.cn (H.Y. Wang)

^bJiangsu Innovation Environmental Engineering Co., Ltd., Yixing, Jiangsu CN214200, China, emails: shaodp@yxcxhb.com (D.P. Shao), pangq@yxcxhb.com (G.Q. Pan)

Received 14 March 2021; Accepted 8 June 2021

ABSTRACT

In this study, water-soluble graphitic carbon nitride nanosheets (WS-CNNS) were successfully prepared by using the KOH/NaOH melt, and the synthesized WS-CNNS could be applied to the environmental treatment. The photocatalytic degradation experimental results showed that the WS-CNNS has great photocatalytic activity for photocatalytic degradation of Methylene blue (MB). Moreover, the capture experiments shown that H₂O₂ played an important role in the photocatalytic degradation of MB. The superior photocatalytic performance of WS-CNNS was mainly ascribed to the characteristics of water solubility together with optical properties. This research provides a new perspective for the application of graphitic carbon nitride nanosheets in environmental remediation.

Keywords: Environmental treatment; Water-soluble; Graphitic carbon nitride; Photocatalytic degradation

1. Introduction

Environmental problems have become more and more serious, which has attracted extensive attention [1–3]. It is urgent to seek an effective technology for environmental remediation. As an advanced oxidation process, photocatalysis is an environmentally friendly route for the treatment of organic pollutants [4–8].

Graphitic carbon nitride (GCN) is widely concerned as an attractive visible-light photocatalyst because of its positive features, including abundance, nontoxicity, stability and narrow bandgap [9–13]. However, GCN suffers from the low surface area and the limited light absorption, which greatly limited the photocatalytic performance [14–16]. For improving the photocatalytic activity of GCN, many modification methods have been proposed (such as

morphology modification, doping and heterostructure construction) [17–19]. Among them, fabricating the nanosheets has been confirmed to be an effective route to improve the photocatalytic activity of GCN [20,21]. However, the conventional methods for the time-consuming multi-step synthesis and low yields, which greatly limited practical applications [22,23]. Recently, Igor et al. [24] prepared water-soluble graphitic carbon nitride nanosheets (WS-CNNS) by using the KOH/NaOH melt, which exhibited high photocatalytic activity and selectivity. Unfortunately, to the best of our knowledge, there is few literature on the application of WS-CNNS in the field of environmental remediation.

Herein, we used the WS-CNNS for environmental treatment. The WS-CNNS showed improved photocatalytic efficiency for the degradation of Methylene blue (MB) compared with that of GCN. Moreover, H₂O₂ played an

* Corresponding author.

important role in the photocatalytic degradation of MB. This research provides a new perspective for the application of GCN nanosheets in environmental remediation.

2. Experimental

2.1. Chemicals

Melamine was obtained from Sinopharm Chemical Reagent Co., Ltd., (China). Methylene blue (MB) was received from Aladdin Industrial Inc. Sodium hydroxide (NaOH) and potassium hydroxide (KOH) were purchased from Sigma-Aldrich Co. LLC. Sodium sulfate (Na_2SO_4) was purchased from Energy Chemical. All chemicals were analytical grade and used without further purification.

2.2. Synthesis of GCN and WS-CNNS

Bulk GCN was obtained by a one-step thermal polymerization of melamine. Specifically, a certain amount of melamine was placed in a covered porcelain crucible and heated to 550°C at a rate of $5^\circ\text{C}/\text{min}$ and maintained at that temperature for 2 h. Finally, a light-yellow powder of bulk GCN was collected by centrifugation, washed with ultrapure water and ethanol, and dried in the oven at 60°C overnight.

For WS-CNNS, a mixture of KOH, NaOH and melamine was heated in a covered crucible at a rate of $5^\circ\text{C}/\text{min}$ up to 360°C and maintained at that temperature for 2 h. The obtained solid was collected by centrifugation, washed with 1.0 M Na_2SO_4 aqueous solution until neutral, and dried in the oven at 60°C overnight.

2.3. Characterization

The morphology of the materials was inspected with a Quanta 250 FEG scanning electron microscope (SEM). The X-ray diffraction (XRD) patterns of the catalysts were obtained by a Bruker-AXS D8 Advance Instrument (Bruker, Germany). Fourier-transform infrared (FT-IR) spectroscopy experiments were performed on a Nicolet iS10 spectrometer. X-ray photoelectron spectrum (XPS) and valence band spectra of the materials were analyzed by an EscaLab250Xi spectrometer using a monochromatic Al K α radiation X-ray source.

2.4. Photocatalytic activity tests

The photocatalytic degradation experiments were tested by degradation of MB (10 ppm) using a 500 W Xenon lamp acting as a light source. In a typical experiment, 20 mg photocatalysts and 50 mL MB solution were put in a quartz tube reactor and thoroughly stirred uniformly to form a suspension. Then the mixture solution was stirring for 0.5 h in the dark to reach the adsorption–desorption equilibrium before turning on the xenon lamp. After turning on the light, 1 mL of suspension was collected at certain time intervals and the photocatalysts were separated by filtration with 0.22 μm . The concentration of MB was detected by the UV-Vis spectrophotometer at the wavelength of 664 nm. To test the stability of photocatalysts, the used photocatalysts were washed with a 1.0 M Na_2SO_4 aqueous solution, dried at 60°C and then recycled.

3. Results and discussion

3.1. Structure and morphology of WS-CNNS

A schematic representation of the synthesis procedure of the WS-CNNS is presented in Fig. 1. The WS-CNNS was obtained by using the KOH/NaOH melt, which reduced the temperature of melamine condensation to GCN structures from the usual range of 500°C – 600°C down to 330°C [24].

XRD patterns were used to analyze the crystallization of WS-CNNS. As presented in Fig. 2a, the diffraction pattern of WS-CNNS exhibited the characteristic peaks of GCN at approximately 13.2° and 27.8° , which corresponded with the (100) and (002) plane of GCN, respectively (JCPDS#871526) [25]. The (100) peak corresponded to in-plane repeated units and the (002) peak corresponded to interlayer reflection of a graphitic-like structure [26].

The chemical structure of WS-CNNS was investigated by FT-IR spectrometry and the results is shown in Fig. 2b. Clearly, The WS-CNNS show characteristic peaks at 815 cm^{-1} , $1,000$ – $1,800\text{ cm}^{-1}$ and $3,185$ – $3,261\text{ cm}^{-1}$, which are attributed to the deformation vibrations of the tri-triazine ring, the typical stretching vibration of C–N heterocyclic ring units and the terminal –NH or – NH_2 groups, respectively [27,28]. Similar features were observed in the spectra of GCN and WS-CNNS, indicating that the two samples had the same main chemical skeletons. This result was consistent with the results of XRD, suggesting that the original atomic structure of GCN was largely retained. Notably, some new peaks appeared in the WS-CNNS except for the characteristic peaks of GCN. The peak at $3,450\text{ cm}^{-1}$ may be assigned to the stretching vibrations of OH $^-$ groups incorporated into the poly(heptazine imide) structure as a result of the alkali melt treatment. Additionally, the peaks appeared in the range $2,150$ – $2,175\text{ cm}^{-1}$ may be assigned to the $\nu(\text{C}\equiv\text{N})$ vibrations [24].

The microstructure and morphology of as-prepared WS-CNNS were investigated by transmission electron microscopy (TEM). As shown in Fig. 3a, the WS-CNNS appears as a 2D sheet-like structure. Moreover, the high-magnification SEM image of the WS-CNNS also clearly exhibited the graphene-like layered structure (Fig. 3b), suggesting that the sheet-like structure of GCN was largely retained. Furthermore, the BET surface area of the WS-CNNS was $28.01\text{ m}^2\text{ g}^{-1}$, which was 2.6 times as high as that of GCN ($22.21\text{ m}^2\text{ g}^{-1}$), supporting the results of TEM.

XPS was further used to analyze the elemental composition and chemical state of the obtained WS-CNNS photocatalysts. As shown in Fig. 4a, the survey XPS spectra verified that WS-CNNS photocatalysts were composed of K, Na, C, N and O [24,29]. The high-resolution spectra of K, C, N, Na and O level for WS-CNNS are shown in

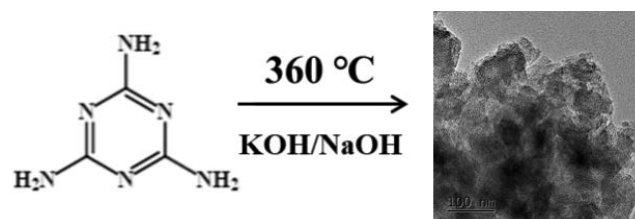


Fig. 1. Schematic illustration of the preparation of WS-CNNS.

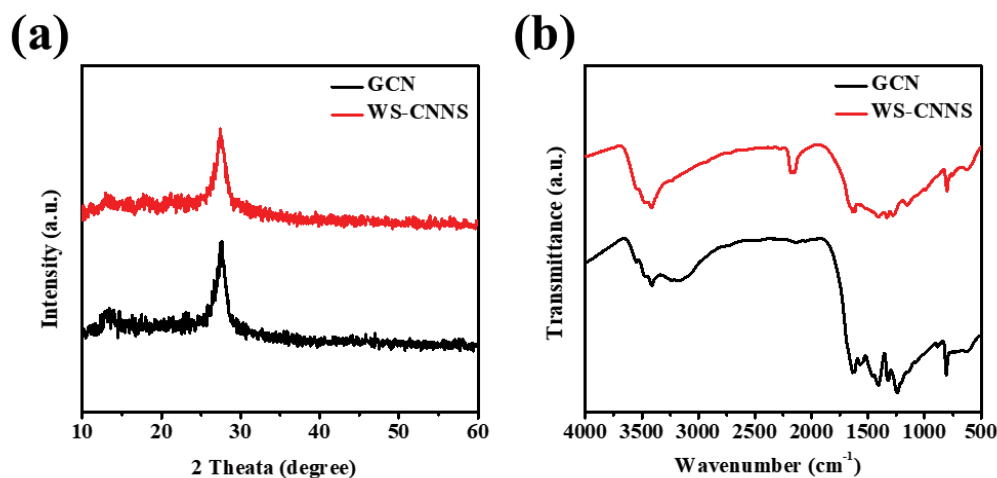


Fig. 2. (a) XRD patterns and (b) FT-IR spectra of GCN and WS-CNNS.

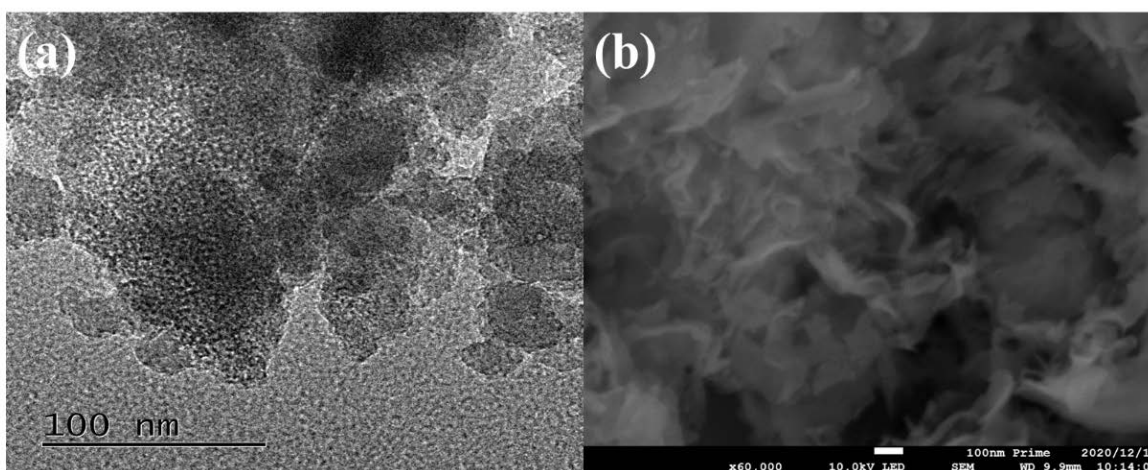


Fig. 3. (a) TEM image and (b) SEM picture of WS-CNNS.

Fig. 4b–e. As shown in Fig. 4b, the high-resolution spectra of the C 1s level for WS-CNNS was deconvoluted to three components including the aromatic carbon atoms (284.6 eV), the C–O[−] groups (286.3 eV) and the sp²-bonded carbon in N=C–N (286.8 eV) [30]. The N 1s high-resolution XPS spectra of WS-CNNS presents three peaks at about 397.1, 398.3 and 399.5 eV, which can be assigned to the C–N=C plus C≡N, the N–C₃ plus triazine C–NH_x and the heptazine C–NH_x, respectively (Fig. 4c) [31]. Notably, the O1s spectrum exhibits a band at 531.0 eV, which can be tentatively assigned to CO₂ chemisorbed by the alkali metal ions (Fig. 4e) [24,32]. Furthermore, the estimated molar ratios of C–N in WS-CNNS according to XPS analysis was 12.6, indicating that WS-CNNS was poor in nitrogen and rich in carbon.

3.2. Photochemical properties of WS-CNNS photocatalysts

The light absorption range and capability of the WS-CNNS photocatalysts were examined by ultraviolet-visible diffuse reflectance spectrum (UV-Vis DRS). In contrast

to GCN, WS-CNNS shows slight blue shifts of the intrinsic absorption edge compared with that of GCN due to the quantum size effect (Fig. 5a). The WS-CNNS presented with a lighter yellow color than that of the GCN. Based on the Kubelka–Munk method, the corresponding bandgaps of GCN and WS-CNNS were determined to be 2.73 eV and 2.03 eV, respectively (Fig. 5b and c) [33,34].

The effective separation of the photo-generated charge carriers is necessary for photocatalysis. The photo-generated charge carriers transfer behaviors were investigated by Photoluminescence (PL). As shown in Fig. 5d, the intensity of PL in WS-CNNS decreased markedly compared with that of GCN, indicating the higher separation efficiency of photo-generated carriers and the narrower bandgap [35]. The narrowed bandgap was consistent with the results from UV-Vis. Transient photocurrent responses and electrochemical impedance spectroscopy (EIS) measurements were further conducted to investigate the photo-generated charge carriers transfer behaviors. Fig. 6a displays the transient photocurrent response of GCN and WS-CNNS. Clearly, WS-CNNS shows the higher photocurrent response,

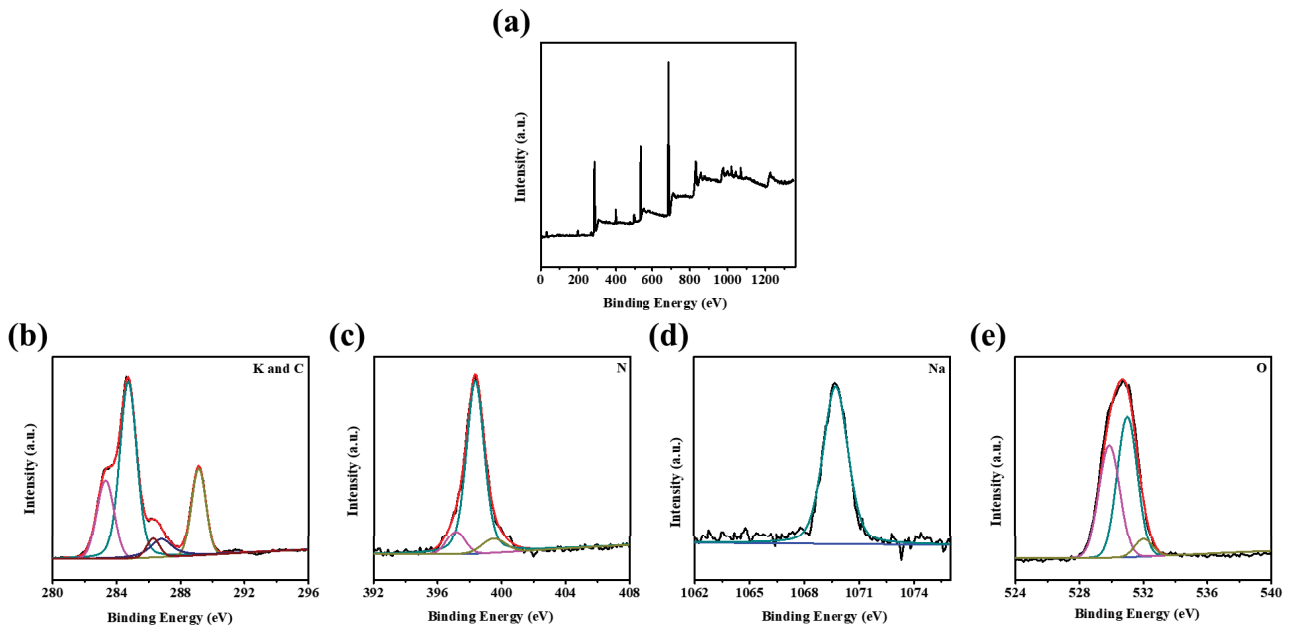


Fig. 4. (a) The survey XPS spectrum of WS-CNNS. C and K (b), N (c), Na (d) and O (e) XPS spectra of WS-CNNS.

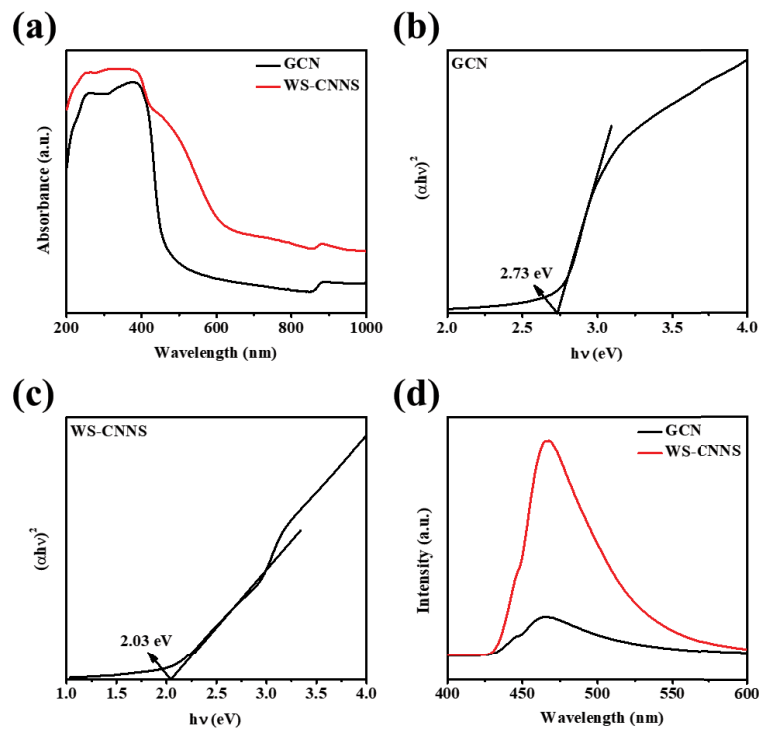


Fig. 5. (a) UV-Vis diffuse reflectance spectroscopy for GCN and WS-CNNS. The bandgap energy (E_g) for GCN (b) and WS-CNNS (c). (d) PL spectra of GCN and WS-CNNS.

indicating that the recombination efficiency of charge carriers was significantly inhibited. Moreover, an obvious decrease in the semicircular Nyquist plots for WS-CNNS over GCN (Fig. 6b), which was consistent with the results of transient photocurrent responses.

3.3. Photocatalytic activities of WS-CNNS photocatalysts

The photocatalytic degradation of MB was used as a model reaction to verify the photocatalytic performance of the resultant WS-CNNS as depicted in Fig. 7a. Clearly, the natural photolysis of MB is negligible in the absence of

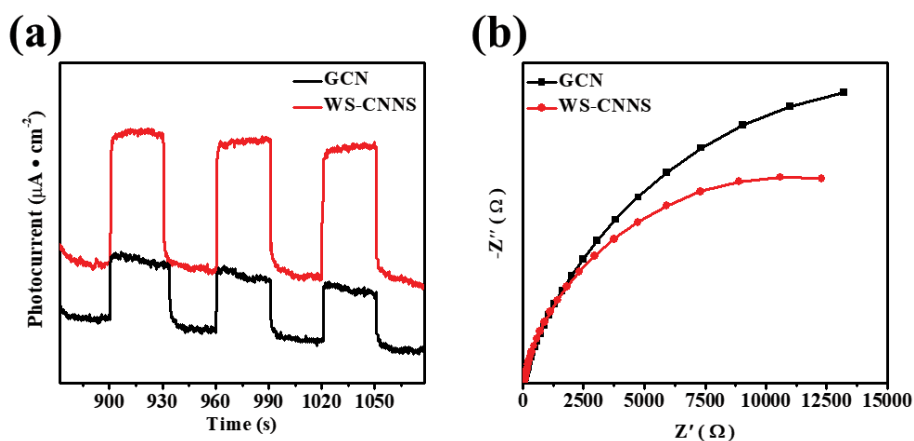


Fig. 6. (a) Transient photocurrent response and (b) EIS Nyquist plots in the dark of the GCN and WS-CNNS.

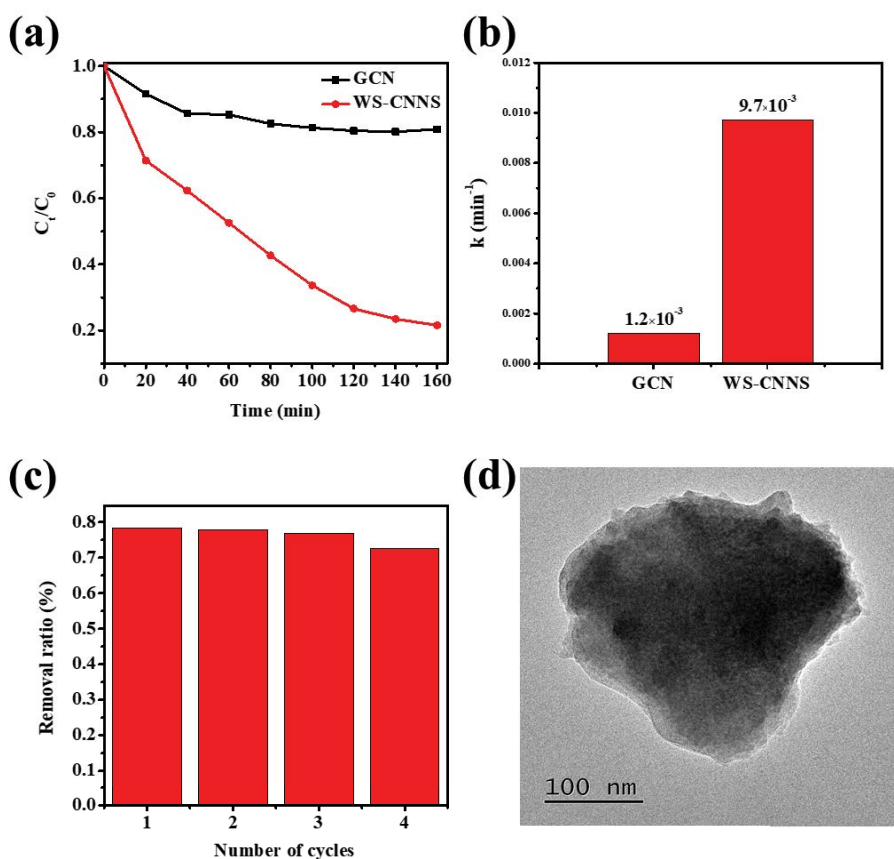


Fig. 7. (a) MB degradation and (b) the pseudo-first-order kinetics data for the photocatalytic degradation of MB by GCN and WS-CNNS under visible light irradiation. (c) Cycling runs for the degradation over WS-CNNS. (d) TEM image of WS-CNNS before reaction and after the 4th recycling reaction.

photocatalysts, indicating the high stability of MB under visible light irradiation. Compared with GCN, the WS-CNNS demonstrated higher degradation efficiencies. Moreover, the photocatalytic activities were further compared by the degradation kinetics and the photo-degradation of MB on WS-CNNS could be well described by the first-order kinetic and the pseudo-first-order kinetics data

for the photocatalytic degradation of MB is shown in Fig. 7b [36]. Apparently, the WS-CNNS demonstrated the higher rate constant compared with that of the GCN. This result is consistent with that of the degradation efficiencies.

To investigate the stability of the WS-CNNS, a repeated experiment with four cycles of photocatalytic MB degradation was performed. As displayed in Fig. 7c, the WS-CNNS

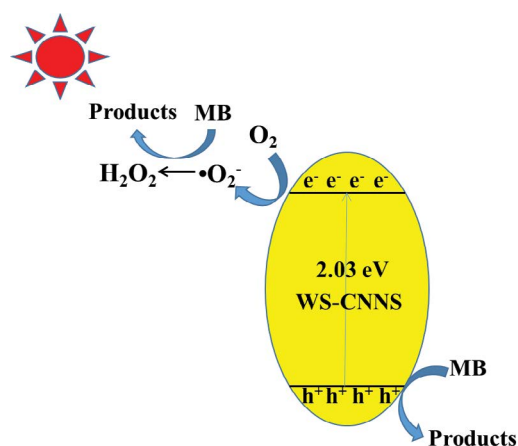
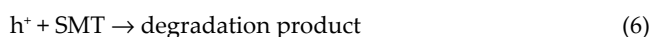
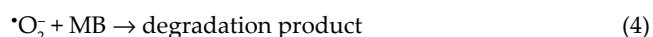
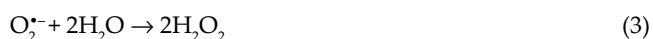


Fig. 8. Schematic illustration of simultaneous degradation of MB over WS-CNNS under visible light irradiation.

retained the superior photocatalytic MB degradation performance after four recycles experiments. Compared with the fresh WS-CNNS, the morphology of the WS-CNNS used did not change significantly (Fig. 7d), indicating the excellent reusability and photocatalytic stability [37].

3.4. Photocatalytic enhancement mechanism

The photocatalytic reaction responsible for the MB degradation might involve surface reactions and the production of reactive species. Species trapping experiments were further performed to confirm active species during the photocatalytic degradation of MB over WS-CNNS. The scavenger of Fe(II)-EDTA were added to trap H_2O_2 . The photocatalytic degradation rate of MB over WS-CNNS was significantly decreased to 63.4% when the Fe(II)-EDTA was added, suggesting that H_2O_2 played an important role in the photocatalytic degradation of MB. A probable mechanism for the improved photocatalytic activity of WS-CNNS for photocatalytic degradation MB is schematically illustrated in Fig. 8 and the possible photocatalytic reaction processes were listed as follows [38]:



4. Conclusions

WS-CNNS was successfully prepared by using the KOH/NaOH melt, and the synthesized WS-CNNS could be applied to the photocatalytic degradation of MB.

The photocatalytic degradation experimental results showed that the WS-CNNS has great photocatalytic activity for photocatalytic degradation of MB. Moreover, the capture experiments shown that H_2O_2 played an important role in the photocatalytic degradation of MB. This article reveals that WS-CNNS had potential to be a promising material in the field of environmental remediation.

Acknowledgements

Thanks to Jiangsu Province scientific and technological achievements into a special fund project (BA2018004) for the support on this work.

References

- [1] R. Ma, S. Zhang, T. Wen, P.C. Gu, L. Li, G.X. Zhao, F.L. Niu, Q.F. Huang, Z.W. Tang, X.K. Wang, A critical review on visible-light-response CeO_2 -based photocatalysts with enhanced photooxidation of organic pollutants, *Catal. Today*, 335 (2019) 20–30.
- [2] Z. Xie, W. Xu, X. Cui, Y. Wang, Recent progress in metal-organic frameworks and their derived nanostructures for energy and environmental applications, *ChemSusChem*, 10 (2017) 81645–1663.
- [3] L. Dong, X. Tong, X. Li, J. Zhou, S. Wang, B. Liu, Some developments and new insights of environmental problems and deep mining strategy for cleaner production in mines, *J. Cleaner Prod.*, 210 (2019) 1562–1578.
- [4] F. Zhang, X. Wang, H. Li, C. Liu, Y. Wan, Y. Long, Z. Cai, Recent advances and applications of semiconductor photocatalytic technology, *Appl. Surf. Sci.*, 9 (2019) 2489, doi: 10.3390/app9122489.
- [5] P. Singh, A. Borthakur, A review on biodegradation and photocatalytic degradation of organic pollutants: a bibliometric and comparative analysis, *J. Cleaner Prod.*, 196 (2018) 1669–1680.
- [6] C. Li, Y. Xu, W. Tu, G. Chen, R. Xu, Metal-free photocatalysts for various applications in energy conversion and environmental purification, *Green Chem.*, 19 (2017) 882–899.
- [7] A. Habibi-Yangjeh, S. Asadzadeh-Khaneghah, S. Feizpoor, A. Rouhi, Review on heterogeneous photocatalytic disinfection of waterborne, airborne, and foodborne viruses: can we win against pathogenic viruses?, *J. Colloid Interface Sci.*, 580 (2020) 503–514.
- [8] S. Asadzadeh-Khaneghah, A. Habibi-Yangjeh, $g\text{-C}_3\text{N}_4$ /carbon dot-based nanocomposites serve as efficacious photocatalysts for environmental purification and energy generation: a review, *J. Cleaner Prod.*, 276 (2020) 124319, doi: 10.1016/j.jclepro.2020.124319.
- [9] F. Guo, M. Li, H. Ren, X. Huang, K. Shu, W. Shi, C. Lu, Facile bottom-up preparation of Cl-doped porous $g\text{-C}_3\text{N}_4$ nanosheets for enhanced photocatalytic degradation of tetracycline under visible light, *Sep. Purif. Technol.*, 228 (2019) 115770, doi: 10.1016/j.seppur.2019.115770.
- [10] C. Wen, J. Li, W. Cen, Y. Sun, S. Lee, F. Dong, Steering the interlayer energy barrier and charge flow via bioriented transportation channels in $g\text{-C}_3\text{N}_4$: enhanced photocatalysis and reaction mechanism, *J. Catal.*, 352 (2017) 351–360.
- [11] J. Wang, Y. Hou, F. Feng, W. Wang, W. Shi, W. Zhang, Y. Li, H. Lou, C. Cui, A recyclable molten-salt synthesis of B and K co-doped $g\text{-C}_3\text{N}_4$ for photocatalysis of overall water vapor splitting, *Appl. Surf. Sci.*, 537 (2021) 148014, doi: 10.1016/j.apsusc.2020.148014.
- [12] A. Akhundi, A. Badiie, G. Ziarani, A. Habibi-Yangjeh, M.J. Muñoz-Batista, R. Luque, Graphitic carbon nitride-based photocatalysts: toward efficient organic transformation for value-added chemicals production, *Mol. Catal.*, 488 (2020) 110902, doi: 10.1016/j.mcat.2020.110902.
- [13] A. Akhundi, A. Habibi-Yangjeh, M. Abitorabi, S.R. Pouran, Review on photocatalytic conversion of carbon dioxide to

- value-added compounds and renewable fuels by graphitic carbon nitride-based photocatalysts, *Catal. Rev.*, 61 (2019) 595–628.
- [14] S. Zhang, P. Gu, R. Ma, C. Luo, T. Wen, G. Zhao, W. Cheng, X. Wang, Recent developments in fabrication and structure regulation of visible-light-driven g-C₃N₄-based photocatalysts towards water purification: a critical review, *Catal. Today*, 335 (2019) 65–77.
- [15] Y. Li, M. Zhou, B. Cheng, Y. Shao, Recent advances in g-C₃N₄-based heterostructured photocatalysts, *J. Mater. Sci. Technol.*, 56 (2020) 1–17.
- [16] S. Cao, B. Fan, Y. Feng, H. Chen, F. Jiang, X. Wang, Sulfur-doped g-C₃N₄ nanosheets with carbon vacancies: general synthesis and improved activity for simulated solar-light photocatalytic nitrogen fixation, *Chem. Eng. J.*, 353 (2018) 147–156.
- [17] S. Cao, H. Chen, F. Jiang, X. Wang, Nitrogen photofixation by ultrathin amine-functionalized graphitic carbon nitride nanosheets as a gaseous product from thermal polymerization of urea, *Appl. Catal., B*, 224 (2018) 222–229.
- [18] X.G. Ma, Y.H. Lv, J. Xu, Y.F. Liu, Y.F. Zhu, A strategy of enhancing the photoactivity of g-C₃N₄ via doping of nonmetal elements: a first-principles study, *J. Phys. Chem. C*, 116 (2012) 23485–23493.
- [19] L. Pan, S. Cao, R. Liu, H. Chen, F. Jiang, X. Wang, Graphitic carbon nitride grown in situ on aldehyde-functionalized a-Fe₂O₃: all-solid-state Z-scheme heterojunction for remarkable improvement of photo-oxidation activity, *J. Colloid Interface Sci.*, 548 (2019) 284–292.
- [20] Y. Wang, Q. Xia, X. Bai, Z. Ge, Q. Yang, C. Yin, S. Kang, M. Dong, X. Li, Carbothermal activation synthesis of 3D porous g-C₃N₄/carbon nanosheets composite with superior performance for CO₂ photoreduction, *Appl. Catal., B*, 239 (2018) 196–203.
- [21] L.R. Yang, X.Y. Liu, Z.G. Liu, C.M. Wang, G. Liu, Q.L. Li, X.X. Feng, Enhanced photocatalytic activity of g-C₃N₄ 2D nanosheets through thermal exfoliation using dicyandiamide as precursor, *Ceram. Int.*, 44 (2018) 20613–20619.
- [22] P.J. Yang, H.H. Qu, Y.X. Fang, X.C. Wang, A facile steam reforming strategy to delaminate layered carbon nitride semiconductors for photoredox catalysis, *Angew. Chem. Int. Ed.*, 56 (2017) 3992–3996.
- [23] F.X. Cheng, H.N. Wang, X.P. Dong, The amphoteric properties of g-C₃N₄ nanosheets and fabrication of their relevant heterostructure photocatalysts by an electrostatic re-assembly route, *Chem. Commun.*, 51 (2015) 7176–7179.
- [24] K. Igor, M. Dariusz, A. Christiane, I. Marina, S. Mariana, M. Luis, N. Christof, T. Andrey, C. Li, D. Benjamin, L. Robert, B. Johannes, K. Ute, C. Im, K. Björn, J. Timo, B. Radim, Water-soluble polymeric carbon nitride colloidal nanoparticles for highly selective quasi-homogeneous photocatalysis, *Angew. Chem. Int. Ed.*, 559 (2020) 487–495.
- [25] S.S. Lu, F.L. Liu, P.X. Qiu, M. Qiao, Y.F. Li, Z.W. Cheng, N.X. Xue, X.K. Hou, C.M. Xu, Y.B. Xiang, F.Q. Peng, Z.B. Guo, Photothermal-assisted photocatalytic degradation with ultrahigh solar utilization: towards practical application, *Chem. Eng. J.*, 379 (2020) 122382, doi: 10.1016/j.cej.2019.122382.
- [26] X.Y. Li, W.H. Xue, S. Dong, E.Z. Liu, Construction of S-scheme Bi₂WO₆/g-C₃N₄ heterostructure nanosheets with enhanced visible-light photocatalytic degradation for ammonium dinitramide, *J. Hazard. Mater.*, 412 (2021) 125217, doi: 10.1016/j.jhazmat.2021.125217.
- [27] H. Wang, B. Chen, K. Song, X.Q. Wang, C.L. Wang, N.Q. Zhao, F. He, Chloroplast-granum-inspired porous nanorods composed of g-C₃N₄ ultrathin nanosheets as visible light photocatalysts for highly enhanced hydrogen production, *Int. J. Hydrogen Energy*, 45 (2020) 2829–2839.
- [28] Q. Zhu, B. Qiu, M. Du, J. Ji, M. Nasir, M. Xing, J. Zhang, Dopant-induced edge and basal plane catalytic sites on ultrathin C₃N₄ nanosheets for photocatalytic water reduction, *ACS Sustainable Chem. Eng.*, 8 (2020) 7497–7502.
- [29] X. Yuan, M. Sun, Y. Yuan, X. Lin, J. Shi, N/Ti³⁺-codoped triphasic TiO₂/g-C₃N₄ heterojunctions as visible-light photocatalysts for the degradation of organic contaminants, *New J. Chem.*, 43 (2019) 2665–2675.
- [30] P. Yang, J.C. Wang, G.Z. Yue, R.Z. Yang, P.X. Zhao, L.J. Yang, X.C. Zhao, D. Astruc, Constructing mesoporous g-C₃N₄/ZnO nanosheets catalyst for enhanced visible-light driven photocatalytic activity, *J. Photochem. Photobiol. A*, 388 (2020) 112169, doi: 10.1016/j.jphotochem.2019.112169.
- [31] X.H. Wang, Z.D. Nan, Highly efficient Fenton-like catalyst Fe-g-C₃N₄ porous nanosheets formation and catalytic mechanism, *Sep. Purif. Technol.*, 233 (2020) 116023, doi: 10.1016/j.seppur.2019.116023.
- [32] S. Cao, H. Chen, F. Jiang, Z.X. Hu, X. Wang, Construction of acetaldehyde-modified g-C₃N₄ ultrathin nanosheets via ethylene glycol-assisted liquid exfoliation for selective fluorescence sensing of Ag⁺, *ACS Appl. Mater. Interfaces*, 10 (2018) 44624–44633.
- [33] Y.J. Liu, H.X. Liu, H.M. Zhou, T.D. Li, L.N. Zhang, A Z-scheme mechanism of N-ZnO/g-C₃N₄ for enhanced H₂ evolution and photocatalytic degradation, *Appl. Surf. Sci.*, 466 (2019) 133–140.
- [34] K. Jiménez-Rangel, J.E. Samaniego-Benítez, L. Lartundo-Rojas, H.A. Calderó, A. Mantilla, Ternary g-C₃N₄/NiOOH/Ag nanocomposite photocatalyst with efficient charges separation and high activity for H₂ production, *Fuel*, 280 (2020) 118672, doi: 10.1016/j.fuel.2020.118672.
- [35] J. Xu, L.W. Zhang, R. Shi, Y.F. Zhu, Chemical exfoliation of graphitic carbon nitride for efficient heterogeneous photocatalysis, *J. Mater. Chem. A*, 1 (2013) 14766–14772.
- [36] S. Cao, Y. Zhang, N.N. He, J. Wang, H. Chen, F. Jiang, Metal-free 2D/2D heterojunction of covalent triazine-based frameworks/graphitic carbon nitride with enhanced interfacial charge separation for highly efficient photocatalytic elimination of antibiotic pollutants, *J. Hazard. Mater.*, 391 (2020) 122204, doi: 10.1016/j.jhazmat.2020.122204.
- [37] P.F. Wang, Y. Liu, N. Jiang, R.S. Jing, S.T. Li, Q. Zhang, H.Q. Liu, J.S. Xiu, Z. Li, Y.Y. Liu, Double S-scheme AgBr heterojunction co-modified with g-C₃N₄ and black phosphorus nanosheets greatly improves the photocatalytic activity and stability, *J. Mol. Liq.*, 329 (2021) 115540, doi: 10.1016/j.molliq.2021.115540.
- [38] S. Cao, Z. Jiao, H. Chen, F. Jiang, X. Wang, Carboxylic acid-functionalized cadmium sulfide/graphitic carbon nitride composite photocatalyst with well-combined interface for sulfamethazine degradation, *J. Photochem. Photobiol. A*, 364 (2018) 22–31.